Designing Climate-Resilient School Playgrounds: A Microclimatic Case Study of Outdoor Thermal Stress in a Mediterranean City (Coimbra, Portugal)

Projetar Pátios Escolares Resilientes ao Clima: Estudo de Caso Microclimático do Stress Térmico Exterior numa Cidade Mediterrânica (Coimbra, Portugal)

Joaquim Francisco P. Fialho [*1], **José Miguel Lameiras** [**2], **Carolina Coelho** [***3] **and António M. Rochette Cordeiro** [****4]

[1]*Faculty of Arts and Humanities, University of Coimbra, 3004-504 Coimbra, Portugal*
[2]*Faculty of Sciences, University of Porto, 4169-007 Porto, Portugal, BIOPOLIS/CIBIO-Research Centre in Biodiversity and Genetic Resources, 4485-661 Vairão, Portugal*
[3]*Faculty of Psychology and Education Sciences, University of Coimbra, 3000-115 Coimbra, Portugal, Center for Interdisciplinary Studies (CEIS20), 3000-186 Coimbra, Portugal*
[4]*Faculty of Arts and Humanities, University of Coimbra, 3004-504 Coimbra, Portugal, Center for Interdisciplinary Studies (CEIS20), 3000-186 Coimbra, Portugal*

Abstract

Outdoor thermal comfort in Mediterranean school playgrounds is increasingly compromised by climate change, 20th-century morphological legacies, and inadequate vegetation planning. This study quantifies outdoor thermal conditions at José Falcão Secondary School (Coimbra, Portugal) using the SOLWEIG (SOlar and LongWave Environmental Irradiance Geometry) microclimatic model within the UMEP framework. High-resolution LiDAR-derived morphology (0.3 m) and in-situ meteorological forcing for 9 May 2024 supported hourly simulations of mean radiant temperature (T_{mrt}), Universal Thermal Climate Index (UTCI), and ground surface temperature (Ts) across nine Points of Interest. Results reveal a daily-averaged T_{mrt} range of nearly 25 °C between dense canopies (≈ 31 °C beneath *Eriobotrya japonica* and *Tilia spp.*) and the asphalt sports field (≈ 51 °C). The pooled regression $UTCI = 15.43 + 0.349 \cdot T_{mrt}$ ($R^2 = 0.94$) demonstrates that, under clear-sky conditions, T_{mrt} statistically accounts for 94% of intra-site UTCI variability. Asphalt sports areas exceed the 55 °C cutaneous burn-risk threshold for three consecutive hours and accumulate up to 11 hours of strong-to-very-strong heat stress. Hence, a clear accessibility paradox emerges: the most thermally favourable spaces remain off-limits to students

*Email: jfpfialho@student.uc.pt
**Email: jmlameiras@fc.up.pt
***Email: carolina.coelho@uc.pt
****Email: rochettecordeiro@fl.uc.pt

Cadernos de Geografia

doi: https://doi.org/10.14195/0871-1623_53_6

Received on: May 8, 2025
Accepted on: July 1, 2026

during school hours, who are concentrated in the most exposed areas. Findings support a hybrid green–grey adaptation strategy combining the opening of existing thermal refugia, asphalt-to-canopy conversion with broadleaved deciduous species, cool-pavement coatings, and vegetated shade structures.

Keywords: Exterior thermal stress. UTCI. SOLWEIG. Mediterranean climate. School playground microclimate.

Resumo

O conforto térmico exterior em pátios escolares mediterrânicos tem vindo a ser progressivamente comprometido pela conjugação das alterações climáticas, das características construtivas do século XX e da insuficiente integração da componente vegetal no desenho dos espaços. O presente estudo procura quantificar as condições térmicas exteriores na Escola Secundária José Falcão (Coimbra, Portugal), mediante a aplicação do modelo microclimático SOLWEIG, integrado na plataforma UMEP. A reconstituição morfológica do sítio, suportada em dados LiDAR de elevada resolução (0,3 m), bem como o forçamento meteorológico observado *in situ* a 9 de maio de 2024, permitiram a simulação horária da temperatura radiante média (T_{mrt}), do Universal Thermal Climate Index (UTCI) e da temperatura da superfície do solo (T^s) em nove Pontos de Interesse. Os resultados obtidos mostram uma amplitude média diária de T_{mrt} da ordem dos 25 °C, contrastando as copas densas (≈ 31 °C sob *Eriobotrya japonica* e *Tilia spp.*) com o campo desportivo asfaltado (≈ 51 °C). A regressão $\text{UTCI} = 15{,}43 + 0{,}349 \cdot T_{mrt}$ ($R^2 = 0{,}94$) demonstra que, sob condições de céu limpo, a T_{mrt} explica, em termos estatísticos, 94% da variância espacial do UTCI. As superfícies asfaltadas do campo desportivo excedem o limiar de risco de queimadura cutânea de 55 °C durante três horas consecutivas, acumulando até onze horas de stress térmico forte a muito forte. Contudo, este caso manifesta um paradoxo de acessibilidade: os espaços termicamente mais confortáveis encontram-se vedados ao uso dos alunos durante o período letivo, pelo que estes se concentram nas áreas mais expostas. Sustenta-se, com base nestes resultados, uma estratégia híbrida verde-cinzenta, articulando a abertura dos refúgios térmicos existentes, a conversão de áreas asfaltadas em zonas arborizadas com espécies caducifólias, a aplicação de revestimentos de elevado albedo e a implementação de estruturas de sombreamento vegetadas.

Palavras-chave: Stress térmico exterior. UTCI. SOLWEIG. Clima mediterrânico. Microclima no pátio escolar.

1. Introduction

School playgrounds are among the most intensively occupied open-air environments in the urban fabric. Children and adolescents typically spend between one quarter and one third of their school day outdoors, often during the central hours of the day when solar forcing is strongest and thermoregulatory capacity is most challenged (Antoniadis et al., 2020; Vanos, 2015). From a bioclimatic standpoint, school playgrounds behave as semi-confined urban canyons in which radiative exchange, surface materiality, and vegetation structure interact to produce highly heterogeneous thermal fields at pedestrian scale (Lai et al., 2020). In Mediterranean climates, these dynamics are intensified by a pronounced seasonal concentration of clear-sky conditions, high solar altitude angles, and increasingly frequent summer heatwaves, which together generate frequent exceedances of outdoor thermal comfort thresholds during regular school activities (Nouri et al., 2024; Silva et al., 2024).

Recent climatological assessments confirm a systematic intensification of heat-related stress across Southern Europe. The IPCC Sixth Assessment Report (IPCC, 2023) attributes the observed increase in heatwave frequency since the mid-20th century to anthropogenic forcing with very high confidence, and projects further amplification under all emission scenarios, with the Mediterranean basin identified as a climate-change hotspot (Cos et al., 2024; Jézéquel et al., 2025; MedECC, 2020). Iberian-scale projections converge on a near-continuous warming and drying signal: heatwave intensity, duration, and spatial extent are all expected to increase by mid-century under both moderate and high-emission pathways (Bento et al., 2025; Lima et al., 2023; Sánchez-Benítez et al., 2025). Within urban areas, these regional signals are further modulated by the urban heat island, whose nocturnal intensity in European cities frequently ranges between 2 and 7 °C and reaches even stronger pedestrian-level radiative contrasts under direct solar exposure (Aroso et al., 2026; Cordeiro, 2023; Yang et al., 2021).

A central insight of recent biometeorological research is that air temperature alone is a poor proxy for outdoor thermal stress. On clear, calm summer days, the radiative environment – captured by mean radiant temperature (T_{mrt}) – explains a substantially greater share of perceived discomfort than near-surface air temperature, which tends to be spatially homogeneous within the canyon-scale (Höppe, 1999; Kántor & Unger, 2011; Lai et al., 2020). Field and modelling studies consistently report that T_{mrt} can exceed 60 °C in sun-exposed paved environments during summer, while shaded vegetated areas may reduce radiative loads by more than 20-30 °C, depending on canopy density, sky view factor (SVF), and leaf area index (Antoniadis et al., 2020; Konarska et al., 2024; Speak et al., 2020). Translating this radiative environment into physiologically meaningful categories has been advanced through the Universal Thermal Climate Index (UTCI), now widely adopted as a standardised metric of outdoor thermal stress (Bröde et al., 2012; Di Napoli et al., 2024).

Resolving these processes at the spatial scale of a schoolyard requires physically based microclimatic modelling. The SOlar and LongWave Environmental Irradiance Geometry (SOLWEIG) model, developed within the Urban Multi-scale Environmental Predictor (UMEP) framework (Lindberg et al., 2018), provides a state-of-the-art, computationally efficient solution for simulating three-dimensional radiative exchange in complex urban geometries. SOLWEIG decomposes the radiative environment around a standing person into six directional components: upward, downward, and four cardinal horizontal orientations; also integrates shortwave and longwave fluxes attenuated by buildings, ground, and vegetation derived from high-resolution digital surface models (Lindberg & Grimmond, 2011; Lindberg et al., 2008). Compared with computationally heavier CFD-based platforms such as ENVI-met, SOLWEIG offers a favourable trade-off between physical realism and the spatial extent that can be simulated at sub-metric resolution, making it particularly well suited to high-density urban settings where LiDAR-derived terrain and canopy data are available (Gholami et al., 2024; UMEP-dev, 2025). Its primary outputs: T_{mrt} and, when coupled with meteorological forcing, UTCI, are widely accepted as biophysical determinants of outdoor thermal comfort. The 2025 implementation of the model further refines vegetation parameterisation through improved canopy transmissivity schemes and a more realistic representation of three-dimensional tree structure, allowing for finer simulation of radiative attenuation in heterogeneous environments (UMEP-dev, 2025).

An equally important conceptual distinction concerns the complementarity between modelled radiative variables and in-situ measurements of air temperature and humidity. Air-temperature data, typically obtained from fixed weather stations or short-duration field campaigns with thermo-hygrometric sensors, characterise the boundary atmospheric forcing but smooth out the radiative heterogeneities that determine pedestrian-level heat exposure (Aroso et al., 2026; Silva et al., 2024). Conversely, model-derived T_{mrt} maps reveal these spatial gradients with metric precision but depend on adequate meteorological forcing for their physiological translation into UTCI (Lindberg et al., 2018; Walikewitz et al., 2015). The coupling of both layers, observed T_a (air temperature) and RH (relative humidity) as boundary conditions, modelled T_{mrt} and UTCI as outcome variables, therefore provides a more complete picture of thermal comfort than either approach in isolation (Pioppi et al., 2024).

Vegetation has consistently been identified as the most effective nature-based strategy for mitigating outdoor thermal stress in cities (Wong et al., 2021; Li et al., 2024). Global syntheses indicate that urban tree canopy cover can reduce near-surface air temperature by 1-5 °C and pedestrian-level UTCI by up to 6-12 °C, predominantly through interception of shortwave radiation rather than direct evaporative cooling (Li et al., 2024; Lai et al., 2020; Speak et al., 2020). Cooling efficacy, however, is highly dependent on structural and physiological traits: leaf area density, canopy porosity, transpiration rate, and spatial configuration and on the background climate. In Mediterranean settings, deciduous broadleaved species offer optimal seasonal performance, providing dense summer shade while allowing winter solar gain after defoliation (Massetti et al., 2019; Rahman et al., 2017). Conversely, evergreens may produce persistent but radiatively less efficient shade if canopy density and ventilation are insufficient, occasionally generating "dry shade" conditions with limited transpirational benefit (Francini et al., 2023; Rötzer et al., 2024).

Despite this consolidated scientific background, a large share of school infrastructures developed during the 20th-century urban expansion of Southern Europe were not designed according to climatic performance principles. In Portugal, this legacy has produced school playgrounds characterised by extensive impermeable surfaces, fragmented vegetation, and limited integration of shading structures (Coelho et al., 2022; Cordeiro et al., 2025). Although contemporary renovation initiatives, notably the *Parque Escolar*[1] programme, have improved indoor energy performance, outdoor environments frequently remain thermally inefficient, particularly during late spring, when student exposure coincides with peak radiative forcing (Cordeiro et al., 2023;

[1] Parque Escolar, is the Portuguese state-owned entity created in 2007 to plan, manage and finance the modernisation and refurbishment of the national public secondary-school building stock. Its interventions have centred mainly on the functional rehabilitation of buildings and on improving indoor conditions and energy efficiency, with comparatively limited attention to the climatic performance of outdoor spaces (Presidência do Conselho de Ministros, 2007).

Riaz et al., 2025). Recent international evidence aligns with this diagnosis: schoolyard ground surfaces in unshaded conditions routinely exceed contact-burn thresholds (≈55 °C) during summer afternoons, while greened or shaded areas remain within tolerable ranges (Pfautsch & Wujeska-Klause, 2022; Sanz-Mas et al., 2025; Vanos et al., 2024).

This building-centred focus reflects a broader tendency in Portuguese facility planning to address collective equipment at the scale of the individual building rather than through an integrated reading of the territory in which it is embedded. Methodologies developed for the territorial planning of networks of collective services and facilities have long argued that such interventions should rest on an integrated geographic and environmental diagnosis (encompassing physical constraints, accessibility, and demographic dynamics), rather than on administrative or building-by-building logics that rarely coincide with the functional and natural boundaries of the territory. Extending this rationale to the school estate implies that the climatic performance of outdoor spaces should be incorporated as an explicit criterion in the diagnosis and programming of school-facility renewal, alongside the indoor and energy-efficiency dimensions that have hitherto prevailed.

Recent research has increasingly addressed this issue through nature-based solutions and participatory design frameworks. Sanz-Mas et al. (2025), evaluating eleven primary schools in Barcelona, demonstrated that combined green-blue-grey interventions (vegetation, water elements, and shade structures), significantly improved heat perception and schoolyard appreciation among children and teachers. The study by Cordeiro et al. (2025), conducted in two secondary schools in Coimbra (Escola Secundária José Falcão, (ESJF), and Escola Secundária D. Dinis, (ESDD), provided a directly relevant local antecedent: combining school-community surveys with thermo-hygrometric measurements, the authors identified a clear correspondence between perceived discomfort and elevated air temperatures over unshaded asphalt surfaces, with up to 5 °C of cooling under tree canopies, and proposed a portfolio of co-designed greening interventions. However, that previous assessment remained primarily perception- and Ta-based, with limited capacity to resolve the radiative processes that dominate pedestrian-level discomfort under clear-sky Mediterranean conditions (Antoniadis et al., 2020; Lai et al., 2020).

The present study extends this research direction by introducing a SOLWEIG-based microclimatic modelling framework to explicitly quantify outdoor thermal conditions in the ESJF schoolyard. Unlike the previous approach, it integrates spatially explicit, hourly simulations of T_{mrt}, UTCI, and ground surface temperature (Ts) at 0.3 m resolution, enabling a mechanistic assessment of thermal exposure patterns driven by urban morphology and surface composition. This allows for the identification of radiative hotspots, the quantification of vegetation-induced cooling effects, and the evaluation of land-cover performance and cutaneous burn risk under representative late-spring conditions. Three guiding research questions structure the analysis: (i) how is the radiative environment spatially distributed across a Mediterranean schoolyard with strong morphological asymmetry? (ii) to what extent does T_{mrt}, rather than air temperature, drive UTCI variability under clear-sky forcing? and (iii) which morphological and vegetation configurations are most effective at reducing radiative exposure and cutaneous burn risk in the spaces most intensively used by students?

By coupling high-resolution SOLWEIG outputs with detailed urban morphology and meteorological data, this study contributes to a more physically grounded understanding of schoolyard microclimates and to evidence-based strategies for climate-adaptive educational environments. It also bridges two methodological traditions – perception and air-temperature-based assessments on one side (Cordeiro et al., 2025; Sanz-Mas et al., 2025), and physically based radiative modelling on the other (Gholami et al., 2024; Lai et al., 2020), by demonstrating how their integration can support the climate-resilient retrofitting of consolidated 20th-century school infrastructures in Mediterranean cities.

2. Geographical Context and Study Site

The city of Coimbra is located in Portugal's central coastal region, occupying a transitional position between the Atlantic coastal lowlands and the elevated inland topography (Figure 1a, b). The prevailing climate exhibits Mediterranean characteristics tempered by Atlantic influences (Ferreira, 2005), manifesting in warm, arid summer months contrasted with mild, precipitation-rich winter periods. Episodic thermal extremes, including both heatwave episodes and cold-air intrusions, occur throughout the year and generate substantial seasonal physiological stress. Urban morphology significantly modulates local thermal patterns: high-density built environments demonstrate elevated nocturnal temperatures consistent with heat-island formation, whereas vegetated corridors and parkland provide ameliorated microclimatic refugia (Cordeiro et al., 2023).

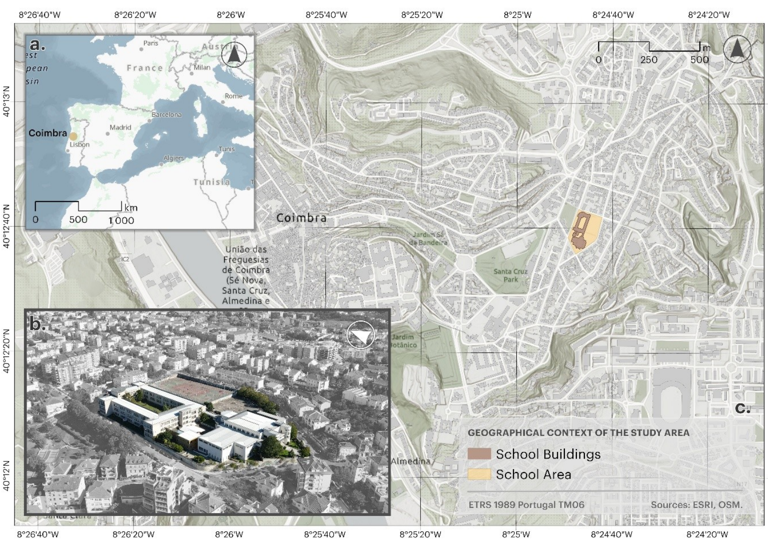

Figure 1. Geographical context of the study area. (a) Location of Coimbra at the European scale; (b) Aerial image of José Falcão Secondary School; (c) Location of José Falcão Secondary School within the city of Coimbra.

José Falcão Secondary School (ESJF) constitutes the primary focus of this investigation. Situated along the eastern hillslope of a compact urban valley in Coimbra's historic core, the institution stands adjacent to the Jardim da Sereia (Figure 1c). The architectural ensemble, completed in 1936 under the direction of Carlos Ramos, Jorge Segurado, and Adelino Nunes, embodies the modernist educational design principles articulated in the "Plano dos Liceus" during Portugal's Estado Novo regime (Moniz, 2007; Nóvoa, 2003). The schoolyard organisation follows the natural topographic gradient through a series of terraced platforms, with the principal spatial element comprising a quadrangular, vegetated central courtyard bounded by learning facilities.

The school's exterior configuration presents a paradox of green-space availability versus accessibility. Despite the presence of multiple vegetated zones – mixed vegetation areas to the northwest and south, a lawn within the main building's central courtyard, and deciduous trees adjacent to the sports field – institutional policies and functional designations render these spaces largely inaccessible to students during regular school hours. The southern vegetated entrance zone is restricted to faculty and extracurricular gymnasium users, whereas the northwestern wooded area serves exclusively as a service zone for cafeteria operations. The central courtyard remains institutionally off-limits. Consequently, student occupation concentrates in the extensive asphalt-surfaced recreation area on the upper terrace and in the covered walkways, both characterised by minimal shade provision and significant solar exposure. The only broadly accessible green amenity comprises a modest stand of linden trees (*Tilia spp.*) bordering the sports court (Figure 1b).

The selection of ESJF as the study location responds to its representative condition within Coimbra's consolidated urban tissue. Embedded within dense 20th-century terrace development and constrained by functionally restricted green infrastructure, the school exemplifies the spatial and environmental challenges confronting heritage educational facilities in established urban centres. This context renders ESJF particularly valuable for examining outdoor thermal comfort dynamics and for evaluating climate adaptation interventions applicable to Portuguese secondary education.

3. Methodology

3.1. Input Data

Urban morphology was reconstructed from airborne LiDAR point clouds (nominal density 10 pts/m^2) acquired in 2024 by the Directorate General for Territory (DGT) and distributed through the National System for Geographic Information (SNIG). All rasters were resampled to 0.3 m ground resolution and projected in ETRS89/PT-TM06 (EPSG:3763). Three elevation surfaces were derived: the Digital Terrain Model (DTM), representing the bare-earth ground elevation; the Digital Surface Model (DSM), representing the elevation of the topmost surfaces, including buildings and tree crowns; and the Canopy Digital Surface Model (CDSM), representing vegetation height above ground and computed as DSM minus DTM for vegetated pixels. The Trunk Zone Surface Model (TDSM) was not generated as an independent raster; instead, a fixed proportion of 25% of the CDSM height was prescribed, following Lindberg and Grimmond (2011), in accordance with the model's standard parameterisation (Figure 3).

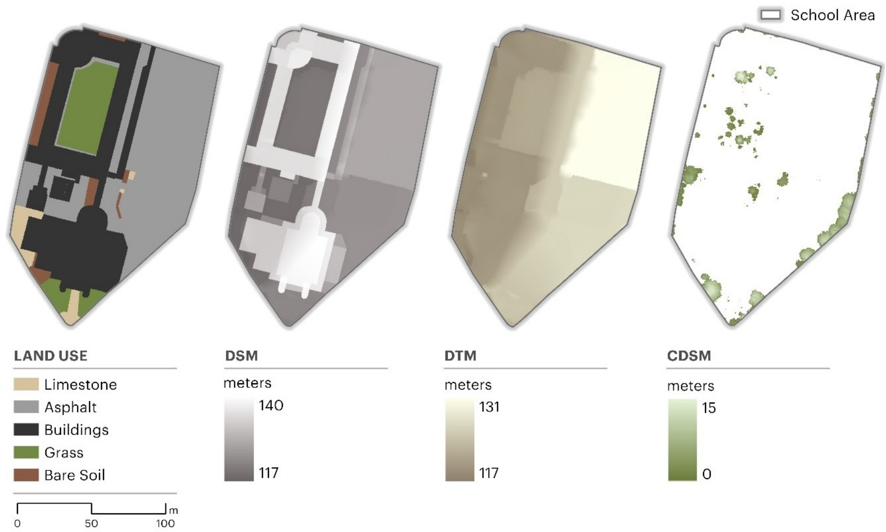

Figure 2. Land-use classification and LiDAR-derived elevation models (DSM, DTM, and CDSM) at 0.3 m.

From these primary surfaces, three additional datasets required by the radiation scheme were computed using the UMEP preprocessing tools: SVF, wall heights, and wall aspect grids. Land cover was manually digitised from 30 cm aerial orthophotography (DGT, 2023), validated against field observations, and reclassified into four surface categories adapted from Lindberg et al. (2018); limestone pavement parameters were adapted from Santamouris et al. (2011) (Table 1). It should be noted that tree canopy is not encoded as a ground land-cover class but volumetrically, through the CDSM and its associated trunk-zone height, in accordance with the SOLWEIG vegetation scheme (Lindberg et al., 2018). The ground beneath each canopy therefore retains its own surface class (e.g., limestone beneath the Loquat stand), while the radiative attenuation of the foliage is resolved separately via the canopy-transmissivity parameterisation; this is why the land-use legend in Figure 3 distinguishes only paved, built and grass surfaces, with the tree layer displayed in the accompanying CDSM panel.

Table 1. Surface radiative properties assigned per land-cover class.

Surface Type	Albedo	Emissivity
Asphalt	0.18	0.95
Bare Soil	0.25	0.94
Buildings	0.20	0.90
Grass	0.16	0.94
Limestone	0.40	0.95

Hourly meteorological data for 9 May 2024 were compiled from multiple sources. Hourly atmospheric pressure was obtained from the Geophysical and Astronomical Observatory of the University of Coimbra (OGAUC), Dias-da-Silva station (n.º 549), located approximately 200 m from the study site. Hourly global horizontal irradiance (Kdn), direct horizontal irradiance (Kdir), and diffuse horizontal irradiance (Kdiff) were retrieved from the Photovoltaic Geographical Information System (PVGIS v5.3), based on the ERA5 reanalysis dataset at the coordinates of the ESJF (Huld et al., 2012). T_a, RH, and wind speed were measured in situ at ESJF following the methodology described in Cordeiro et al. (2025). Briefly, air temperature and relative humidity were recorded with a portable thermo-hygrometric sensor and wind speed with a portable anemometer – LUTRON AM-4214SD–, positioned at pedestrian height (1.5 m) at the study site over the field-campaign period; these in-situ records supplied the boundary atmospheric forcing for the SOLWEIG simulations. During the simulation period, T_a ranged from 21.8 °C (08:00) to 33.7 °C (14:00), RH varied between 21% and 41.9%, and peak global irradiance reached 910.5 W/m^2, corresponding to an anticyclonic regime over the Iberian Peninsula characterised by persistent clear-sky conditions and high global irradiance, both conducive to outdoor thermal stress (Lau et al., 2015). This date was selected as a representative late-spring, clear-sky day under anticyclonic forcing, coincident with the in-situ field campaign and with a period of effective outdoor occupation by students, in order to capture upper-bound radiative contrasts. A late-spring day was deliberately preferred over a peak-summer one because the Portuguese school calendar runs only until mid-June: the hottest months (July and August) fall outside the period of student occupation. A clear-sky early-May day therefore reflects the most adverse radiative conditions actually experienced by students during the school year and provides an upper-bound estimate of in-use thermal exposure, rather than the absolute annual maximum, which would occur when the schoolyard is unoccupied.

3.2. Computation of mean radiant temperature

In SOLWEIG, T_{mrt} is computed by resolving the radiative environment around a standing person into six directional components (upward, downward, and four horizontal orientations). This enables a physically consistent representation of radiative exchange in urban environments with complex geometry (Lindberg & Grimmond, 2011; Lindberg et al., 2008).

Shortwave radiation is decomposed into direct, diffuse, and surface-reflected components, modulated by the SVF and shadowing effects. Anisotropic features of diffuse sky radiation, including circumsolar enhancement and horizon brightening, are explicitly considered. Longwave radiation includes atmospheric emission and terrestrial emission from surrounding urban surfaces, with surface temperatures estimated from a transient heat-balance formulation based on material thermal properties (Jänicke et al., 2024).

The total absorbed radiant flux density (S_{str}) is then converted into T_{mrt} through the Stefan-Boltzmann inversion:

$$T_{\mathrm{mrt}} = \left(\frac{s_{\mathrm{str}}}{\varepsilon_{\mathrm{p}}\,\sigma}\right)^{1/4} - 273.15 \quad (1)$$

where σ is the Stefan-Boltzmann constant and ε_p is the emissivity of the human body. The subtraction of 273.15 represents the unit conversion from Kelvin to degrees Celsius, since the radiative computation is performed on the absolute-temperature scale. All computations are conducted at 1.1 m above ground level, representing pedestrian-level exposure conditions (Lindberg et al., 2008).

3.3. Points of Interest and Thermal Stress Assessment

Nine Points of Interest (POI) were selected across the schoolyard to capture the full spectrum of morphological configurations and surface-cover conditions experienced by students throughout the school day, ranging from fully exposed impervious areas to densely shaded vegetated environments. The selected locations and their defining characteristics are described below (Figure 3):

Sports Field – a large open area on the upper terrace, surfaced in asphalt and devoid of vegetation, with no vertical obstructions in its immediate surroundings except the school wall on the east side; **Sports Court** – a hard-surfaced recreational area, also paved in asphalt, more spatially confined than the Sports Field and bordered by low built elements; **Garden** – an inner courtyard composed of grass and low vegetation, enclosed by the school's building mass, with predominantly permeable surfaces; **South Garden** – vegetated area near the southern entrance, combining grass and scattered trees, with a more open configuration than the central courtyard; **Cafeteria** – outdoor area directly adjacent to the cafeteria building, with asphalt-paved surfaces and proximity to vertical façades; **Shed** – location defined by a small built structure with surrounding impermeable ground cover and immediate adjacency to constructed elements; **Orangery** – limestone-paved area adjacent to a row of orange trees with no canopy overlap or direct shading at pedestrian level; **Loquat** – zone dominated by mature *Eriobotrya japonica*, characterised by dense tree cover and limestone pavement; **Linden** – located along the linear arrangement of *Tilia spp.* on the south-east edge of the sports court.

Figure 3. Location of the POI across the José Falcão Secondary School schoolyard, with land-cover context.

Outdoor thermal stress was assessed using the UTCI, computed in SOLWEIG from T_a, T_{mrt}, wind speed, and humidity, following the standard UTCI formulation (Bröde et al., 2012). UTCI values were categorised according to the standard thermal-stress scale: no stress (9-26 °C), moderate heat stress (26-32 °C), strong heat stress (32-38 °C), very strong heat stress (38-46 °C), and extreme heat stress (>46 °C) (Bröde et al., 2012; Di Napoli et al., 2024).

To quantify the relative thermal benefit provided by each POI, daily mean T_{mrt} and UTCI were compared against those of the Sports Field, an open-field site without shading or morphological obstruction that served as the unobstructed reference condition. Negative differences (ΔT_{mrt}, ΔUTCI) indicate a cooling effect relative to fully exposed conditions.

Additionally, ground surface temperature (T_s) was estimated from the SOLWEIG upwelling longwave flux via the Stefan-Boltzmann equation, assuming a ground emissivity of 0.95. T_s values were evaluated against the 55 °C burn-risk threshold for brief cutaneous contact defined by ASTM C1055-20 (ASTM International, 2020), a criterion of particular relevance for schoolyard environments where adolescent activities frequently involve barefoot contact or direct sitting on ground surfaces (Pfautsch & Wujeska-Klause, 2022).

3.4. Statistical Analysis

All SOLWEIG outputs were extracted at the nine POI, producing a structured dataset of 108 observations (9 POI x 12 hourly time steps). Prior to analysis, data integrity was verified to ensure temporal completeness and internal consistency, with no missing values recorded.

Thermal variables (T_{mrt}, UTCI, Ts) were analysed through descriptive statistics (mean, standard deviation, range) to characterise spatial and temporal variability. Differential thermal indicators (ΔT_{mrt}, ΔUTCI) were computed relative to the Sports Field as the fully exposed reference condition.

A high-resolution sub-daily analysis was performed for the critical period of maximum radiative forcing. The interval between 13:15 and 14:30 was re-simulated at 10-minute temporal resolution for T_{mrt}, in order to capture peak conditions of direct solar incidence and maximum thermal stress, following the methodological approach adopted in previous work (Cordeiro et al., 2025). The resulting high-frequency dataset was used to compute intra-period variability and to quantify cooling performance under peak exposure conditions.

Associations between T_{mrt} and UTCI were evaluated using Pearson's correlation coefficient and ordinary least-squares linear regression. The model was applied to the pooled dataset to assess the sensitivity of thermal stress to radiative forcing under clear-sky conditions. Statistical significance was considered at a confidence level of 95% ($\alpha = 0.05$). Model assumptions – linearity, homoscedasticity, and normality of residuals – were assessed through visual diagnostics. Given the repeated-measures structure of the dataset (multiple POI under identical meteorological forcing), results are interpreted as spatially comparative microclimatic patterns rather than statistically independent samples; mixed-effects or hierarchical modelling was not applied, since the objective is the characterisation of intra-site thermal variability rather than population-level inference.

All statistical processing was conducted using SPSS Statistics v29.0. Spatial data handling and SOLWEIG simulations were performed in QGIS 3.34 LTR with the UMEP plugin (Lindberg et al., 2018); graphical outputs were generated using SPSS Statistics v29.0 (statistical charts and regression plots).

4. Results

4.1. Spatial patterns of mean radiant temperature

The spatial distribution of daily-averaged T_{mrt} across the ESJF schoolyard (Figure 4) reveals a radiative range of nearly 25 °C between the coolest and warmest pixels (27.4-52.3 °C), with a schoolyard-wide mean of 41.5 °C. The northern patches corresponding to small bush gardens were excluded from the analysis due to their limited functional relevance.

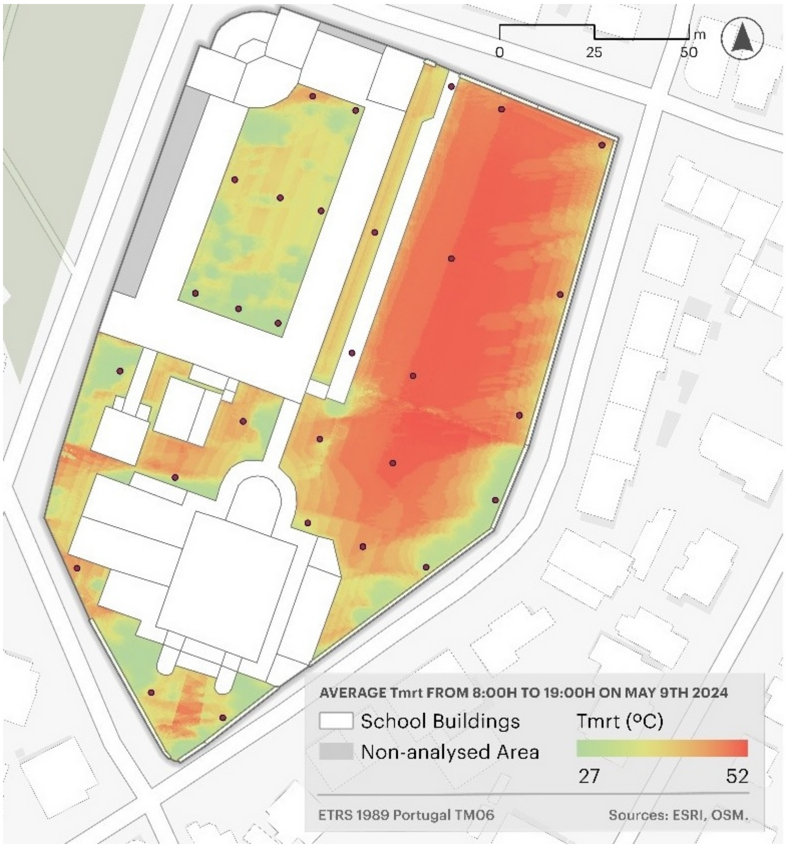

Figure 4. Average T_{mrt} from 08:00 to 19:00 on 9 May 2024 at José Falcão Secondary School.

The most prominent feature is the extensive red-orange zone occupying the eastern sector of the schoolyard, corresponding to the open asphalt recreation field. This area, the only broadly accessible outdoor space for students during break periods, sustains daily mean T_{mrt} values of 49-51 °C at the POI locations (Sports Field: 49.4 °C; Sports Court: 50.7 °C) (Figure 5). The absence of trees, combined with the high solar absorptivity of the asphalt surface, produces persistent radiative exposure from mid-morning through late afternoon, visible as an unbroken warm-toned mass on the map.

In sharp contrast, the north-western vegetated zone – occupied by mature *Eriobotrya japonica* (Loquat), together with the south-eastern stand of *Tilia spp.* – appear as distinctly cooler green patches, with daily mean T_{mrt} of 31.0-31.4 °C at the canopy-shaded POI. This represents a reduction of approximately 18 °C relative to the open field, consistent with over 95% interception of incoming shortwave radiation by the dense deciduous canopy ($\tau = 0.05$). However, this thermally favourable zone is functionally designated as a service area for cafeteria operations and is not accessible to students during the school day.

Between these two extremes, a range of intermediate conditions is visible across the terraced platforms of the schoolyard. The central courtyard, enclosed by the quadrangular building perimeter, exhibits moderate T_{mrt} values (Garden: 37.0 °C), substantially cooler than the open field, reflecting the combined effect of partial vegetation cover and intermittent building shadows. Yet this space, too, remains institutionally off-limits. The transitional zones adjacent to building structures (Cafeteria: 40.3 °C; Shed: 39.8 °C) display the patchy yellow-orange pattern characteristic of spaces where shade coverage is intermittent and dependent on the solar azimuth at each hour.

Linear strips of reduced T_{mrt} are discernible along the northern and western edges of building footprints, corresponding to the cast-shadow corridors generated by the school's multi-storey blocks. These narrow cool bands extend a few metres from the façades and migrate throughout the day with the sun path, offering transient – but not sustained – thermal relief.

The spatial structure of T_{mrt} thus exposes a clear thermal dichotomy within the ESJF schoolyard: the areas of greatest thermal comfort (dense canopy in the northwest, enclosed courtyard) are precisely those to which students have no access, while the only broadly available recreation space (asphalt field) concentrates the highest radiative exposure. The linden trees bordering the small sports field (Linden: 31.4 °C) represent the sole accessible green amenity offering meaningful thermal benefit, but their limited canopy extent is insufficient to serve the wider school community.

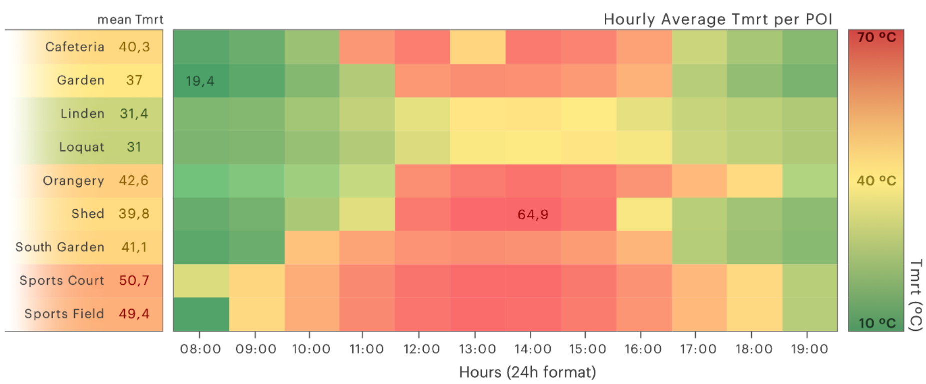

Figure 5. Hourly average T_{mrt} for each Point of Interest (9 POI x 12 h). The maximum value (64.9 °C) was recorded at 14:00 at the Shed location, while the minimum (19.4 °C) occurred at 08:00 in the Garden.

4.2. Diurnal evolution of thermal stress

The hourly evolution of UTCI across the schoolyard (Figure 6) reveals a marked spatial differentiation that emerges with solar elevation. During early morning hours, thermal conditions remain relatively homogeneous, with an inter-site UTCI range of only 4.0 °C at 08:00. As solar radiation intensifies, this range expands rapidly, reaching 7.5 °C by 11:00 and remaining above 7.0 °C until mid-afternoon. By 19:00, the range collapses to 1.7 °C as solar input diminishes. This behaviour confirms that the observed 5.1 °C difference in mean daily UTCI between the coolest (Loquat, 27.2 °C) and warmest (Sports Field, 32.3 °C) locations is largely explained by differences in the radiative environment, while air temperature remains spatially homogeneous across the campus.

Dense canopy sites remain below or near the strong heat-stress threshold (32 °C) for most of the day, whereas open-field locations and the Shed exceed 38 °C during peak hours (13:00-14:00). Two distinct windows of thermally acceptable conditions emerge, early morning (08:00-10:00) and late afternoon (after 17:00), during which all locations remain below the strong-stress threshold.

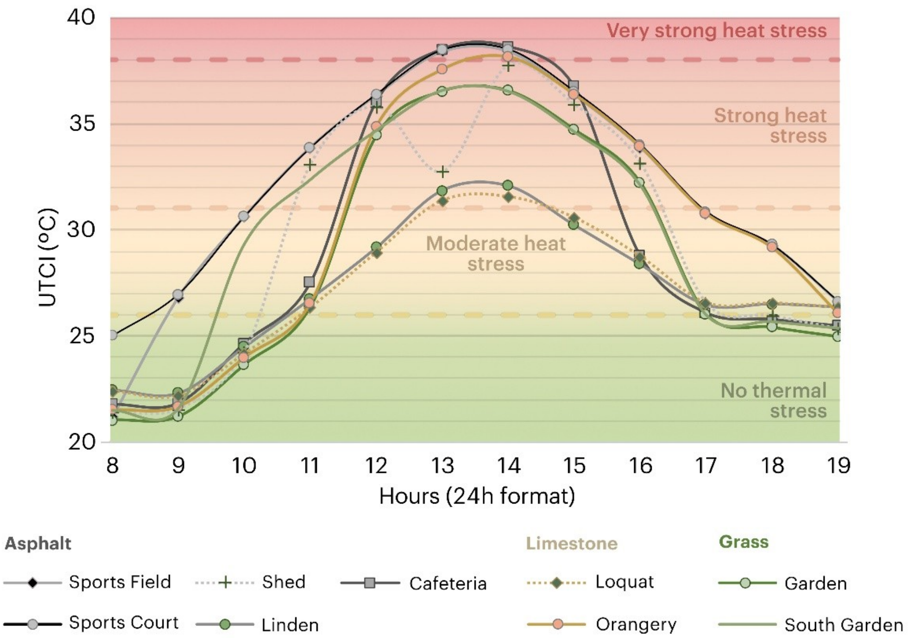

Figure 6. Hourly evolution of UTCI with thermal-stress thresholds at 26, 32, and 38 °C.

4.3. Cumulative thermal stress exposure

The dataset evidences a clear stratification of cumulative thermal-stress exposure across all POI, strongly mediated by canopy cover and spatial configuration. Vegetated sites – particularly Loquat and Linden – demonstrate the most favourable thermal performance, with a complete absence of strong and very strong heat stress and a concentration of exposure within moderate stress (8-9 hours).

In contrast, open and semi-exposed environments such as the Sports Field, Sports Court, and South Garden exhibit substantially higher cumulative thermal stress. These locations register the highest total exposure (11 hours in the sports areas), including 2 hours of very strong heat stress, alongside extended periods of strong stress.

Anomalous behaviour is observed at the Shed, which, despite a comparatively low SVF (0.42), accumulates 2 hours of very strong stress. This performance is unexpectedly poorer than that of the Garden (SVF = 0.68), which records no very strong stress. This suggests that SVF alone is insufficient to fully explain thermal outcomes; additional factors – such as material thermal properties, ventilation constraints, or surrounding radiative feedback – likely contribute to localised heat accumulation.

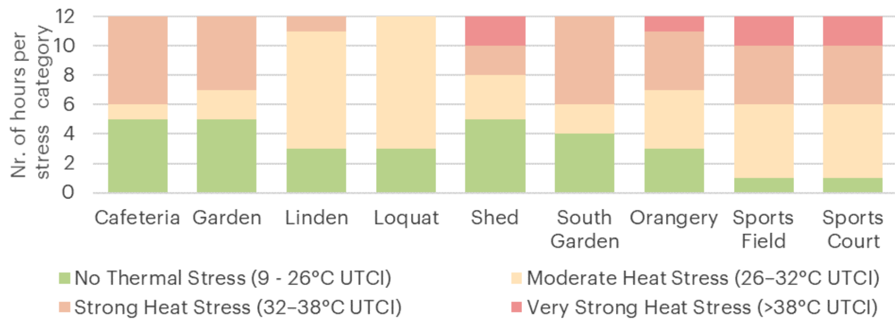

Figure 7. Number of hours per UTCI thermal-stress category at each POI.

4.4. Cooling potential relative to the Sports Field

The cooling potential, expressed as ΔUTCI and ΔT_{mrt}, quantifies the thermal offset of each POI relative to the Sports Field reference during the period of maximum radiative forcing (13:15-14:30 UTC), corresponding to peak incoming global irradiance and the highest sustained thermal stress recorded across the simulation day (Figure 8).

The Loquat and Linden canopies register the largest cooling, with ΔUTCI of -6.51 °C and -6.28 °C and ΔT_{mrt} of -25.92 °C and -25.01 °C, consistent with their shared SVFbv of 0.02 and shadow fraction of 0.03, which attenuate over 93% of incoming shortwave radiation and shift thermal stress from "very strong" to "moderate". The South Garden and Garden present intermediate reductions (ΔUTCI of -1.78 °C and -1.73 °C; ΔT_{mrt} of -7.09 °C and -6.90 °C), attributable to lower surface temperatures over vegetated ground under full sun exposure, while the Cafeteria (-0.23 °C) and Orangery (-0.03 °C) are effectively indistinguishable from the reference – the latter case confirmed by the identity of SVFbv and SVFb (both 0.54), indicating no additional sky obstruction from the existing tree canopy.

The Sports Court and Shed are the only POI where conditions exceed the open-field reference. The Sports Court records a marginal warming (+0.16 °C UTCI;

+0.62 °C T_{mrt}), whereas the Shed presents the highest thermal load in the dataset (+0.38 °C UTCI; +1.50 °C T_{mrt}) accompanied by the maximum Ldown across all sites (517 W/m^2) – its overhead structure reduces SVFb to 0.42 but fails to cast effective shade during the study period, instead trapping and re-emitting longwave radiation downward beyond open-sky levels.

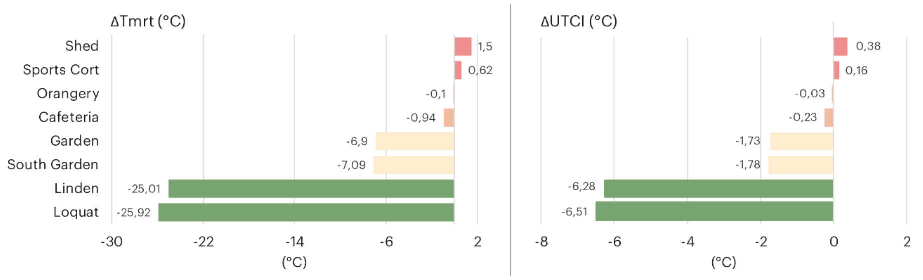

Figure 8. Cooling potential of each POI relative to the Sports Field: ΔUTCI (left) and ΔT_{mrt} (right). Negative values indicate thermal benefit.

4.5. Mean radiant temperature as the main driver of UTCI

The relationship between hourly T_{mrt} and UTCI for the pooled dataset ($n = 108$) reveals a strong and highly significant linear association. The regression model, expressed as $UTCI = 15.43 + 0.349 \cdot T_{mrt}$ ($R^2 = 0.94$, $p < 0.001$), indicates that each 1 °C increase in T_{mrt} corresponds to an approximate rise of 0.35 °C in UTCI. The high correlation coefficient ($r = 0.97$) demonstrates that, under clear-sky conditions, the radiative environment is the primary driver of outdoor thermal stress, whereas air temperature remains spatially homogeneous across all POI at each timestep and thus exerts a comparatively minor influence (Figure 9).

The dispersion of data points along the regression line exhibits a clear spatial structuring. Locations characterised by dense tree canopy, such as the Loquat and Linden sites, form a compact cluster in the lower-left portion of the distribution. These points span a relatively narrow T_{mrt} interval of 14 °C (24-38 °C) and remain below UTCI values of 32 °C. This constrained variability reflects the strong radiative attenuation provided by vegetation, where the interception of more than 95% of incoming shortwave radiation effectively dampens fluctuations in radiant heat load at ground level.

In contrast, exposed areas such as the Sports Field and Sports Court display a much broader distribution, extending across the full range of the regression. These locations experience a T_{mrt} span of approximately 45 °C (20-65 °C), with corresponding UTCI values reaching up to 39 °C. Intermediate environments (Garden, South Garden, Cafeteria, Shed, and Orangery), occupy transitional positions, showing convergence in the early morning and late afternoon, followed by pronounced divergence during periods of peak solar forcing.

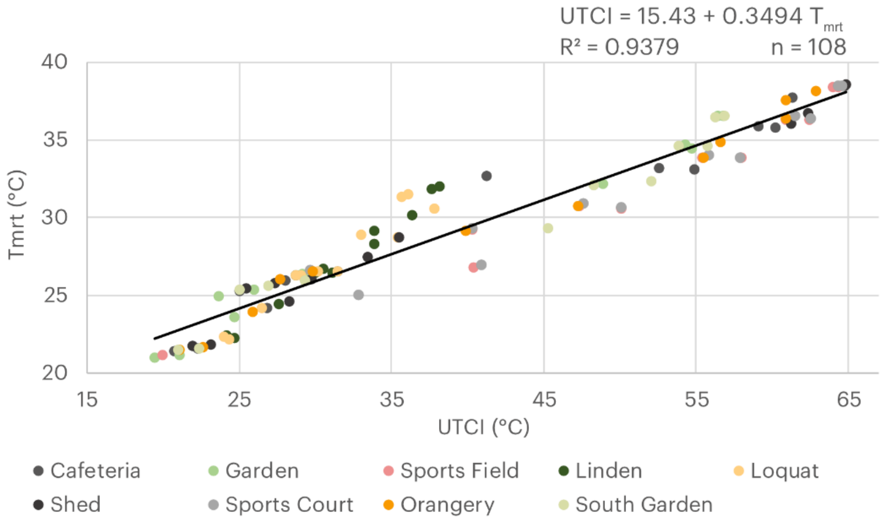

Figure 9. Linear regression between hourly T_{mrt} and UTCI across the nine POI (n = 108). Each series represents a single POI. Fitted equation: UTCI = 15.43 + 0.349 · T_{mrt} (R^2 = 0.9379).

4.6. Ground surface temperature and contact-burn risk

Across the nine POI, Figure 10 depicts the temporal evolution of estimated ground surface temperature (T_s), obtained from the SOLWEIG-simulated upwelling longwave radiation under a ground emissivity of 0.95. The two open-field sites – Sports Field and Sports Court – exceed the 55 °C cutaneous burn-risk threshold defined by ASTM C1055-20 for three consecutive hours between 12:00 and 14:00, peaking at 58.3 °C and 58.4 °C respectively around 14:00. These surfaces correspond to the asphalt-paved recreation areas where student occupation is concentrated during morning and afternoon break periods.

Among the remaining POI, the Shed approaches but does not exceed the threshold (peak T_s = 52.6 °C), followed by the Orangery (49.8 °C) and the Cafeteria (48.7 °C). Garden and South Garden remain below 40 °C, while dense canopy surfaces (Loquat: 36.2 °C; Linden: 35.3 °C) stay below 37 °C throughout the day, with surface temperatures closely tracking the ambient air temperature. The contrast between extremes is pronounced: at 14:00, the ground beneath the Loquat canopy is 22 °C cooler than the asphalt at the Sports Court, a direct consequence of near-total shortwave interception.

The exceedance of the burn-risk threshold in the most heavily used outdoor areas introduces a safety concern that extends beyond thermal comfort. At the recorded surface temperatures, brief barefoot contact or direct sitting on the ground may produce first-degree burns within seconds of exposure (Pfautsch & Wujeska-Klause, 2022). This risk is compounded by the behavioural patterns typical of the school population: adolescents frequently sit directly on ground surfaces during breaks and may engage in physical activities with exposed skin in contact with the pavement.

The spatial coincidence between the highest Ts values and the primary student recreation zone reinforces the case for targeted shading interventions in this sector of the schoolyard.

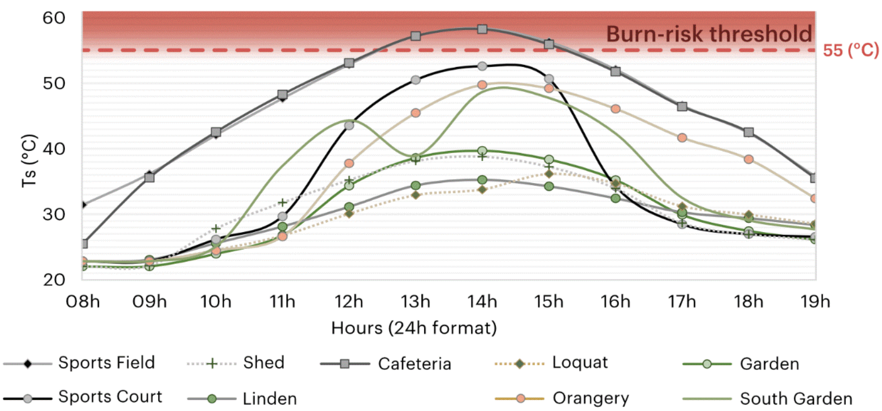

Figure 10. Hourly estimated ground surface temperature across the nine POI. The dashed horizontal line indicates the 55 °C burn-risk threshold for brief cutaneous contact (ASTM C1055-20). Sports Field and Sports Court exceed this threshold for three hours (12:00-14:00).

5. Discussion

5.1. Radiation, not air temperature, drives schoolyard heat stress

The strongest and most consistent finding across the ESJF dataset is the dominance of the radiative environment over air temperature as a driver of pedestrian-level heat stress. The pooled regression $UTCI = 15.43 + 0.349 \cdot T_{mrt}$ ($R^2 = 0.94$; $r = 0.97$) indicates that more than nine tenths of the inter-site variability in UTCI is explained by T_{mrt} alone, while Ta and RH, quasi-uniform across the campus at each timestep, account for the remaining baseline. This empirical decomposition aligns with the broader biometeorological consensus that, under clear, calm summer days, T_{mrt} is the leading meteorological driver of human thermal stress (Höppe, 1999; Kántor & Unger, 2011; Lai et al., 2020) and confirms that Ta is an inadequate substitute for T_{mrt} in the assessment of outdoor comfort (Walikewitz et al., 2015).

This result has direct methodological implications for the previous Coimbra schoolyard study (Cordeiro et al., 2025), which reported a maximum spatial difference of approximately 5 °C in air temperature between unshaded asphalt and tree-shaded zones at ESJF. The present SOLWEIG-based assessment shows that this Ta range, while informative as a boundary condition, captures only a fraction of the actual radiative load to which students are exposed: at 13:15-14:30, the radiative offset (ΔT_{mrt}) between the Loquat canopy and the Sports Field reaches -25.9 °C, which translates into a UTCI offset of -6.5 °C – well above the magnitude that air-temperature measurements alone would suggest. The two methodologies are therefore not redundant but complementary: in-situ Ta and RH measurements characterise the boundary atmospheric forcing, while modelled T_{mrt} resolves the spatial heterogeneity that ultimately governs perceived comfort. This dual-layer approach reinforces and physically grounds the perception-based diagnosis previously reported by the school community (Cordeiro et al., 2025), in which students consistently described the asphalt yard as "unbearable" during midday, despite Ta differences of only a few degrees Celsius.

5.2. The paradox of accessibility: where comfort exists and where students are

The spatial structure of T_{mrt} across ESJF reveals a striking and educationally consequential paradox. The schoolyard contains three thermally favourable environments: the Loquat canopy (daily mean $T_{mrt} \approx 31.0\,°C$); the Linden grove ($\approx 31.4\,°C$); and the central Garden ($\approx 37.0\,°C$); yet two of the three are functionally inaccessible to students during ordinary school hours. The only broadly accessible outdoor space, the asphalt sports field, simultaneously concentrates the highest radiative loads (49-51 °C daily mean T_{mrt}) and the highest cumulative duration of strong-to-very-strong heat stress (11 hours, including 2 hours above the 38 °C UTCI threshold). The Linden stand, the only accessible green amenity, offers genuine thermal benefit but is too small in canopy extent to serve the entire school population during recess.

This pattern was already qualitatively identified in the school-community survey reported by Cordeiro et al. (2025), in which respondents described problem zones (cafeteria, both sports fields and the shed area) as "too hot in summer" and explicitly flagged the locked or restricted green areas (Garden and South Garden) as "missed opportunities to improve both comfort and aesthetics". The present SOLWEIG simulations physically confirm and quantify this perception: the institutional decision to restrict access to the most thermally comfortable areas effectively forces students into the most radiatively hostile sector of the campus during the hottest hours of the day. The mismatch between green-space availability and green-space accessibility emerges, therefore, as a key shortcoming in the spatial organisation of the ESJF outdoor environment: a finding that resonates with the "gap between appreciation in theory and actual usage in practice" reported in Mediterranean school playgrounds more broadly (Sanz-Mas et al., 2025) and with the access-equity dimension increasingly emphasised in green-schoolyard scholarship (Wolf et al., 2024).

5.3. Vegetation performance: canopy density, species, and the limits of evergreens

The cooling hierarchy retrieved by the model is consistent with the morphological and physiological traits of the dominant species. The two best-performing POI – Loquat and Linden – combine high canopy density (shadow fraction ≈ 0.97) with deciduous broadleaved foliage, which offers near-total shortwave interception in summer and seasonal reversibility in winter. Both *Eriobotrya japonica* and *Tilia spp.* are well documented as effective Mediterranean shade species: the former combines moderate transpiration with very dense, persistent foliage during the warm season (Rana et al., 2019), while the latter is among the most extensively validated urban-shade taxa, with demonstrated reductions in pedestrian-level air temperature of up to 0.85 °C and surface-temperature reductions of up to 20 °C under full canopy in Mediterranean and Central-European cities (Massetti et al., 2019; Rahman et al., 2017; Stratópoulos et al., 2024).

By contrast, the Orangery POI, a limestone-paved area positioned next to (rather than beneath) a row of young orange trees, registers a near-zero ΔUTCI (-0.03 °C) and a daily mean T_{mrt} virtually identical to the open Sports Field. The identity of SVFb and SVFbv (both 0.54) confirms that, at the assessed point, no canopy element interposes itself between the pedestrian plane and the sky: the orange trees are still young, with small crowns whose lateral extent does not yet reach the sampling location, and the resulting radiative environment is therefore effectively that of an open paved surface. This finding does not concern the cooling potential of mature orange trees per se, well documented in Mediterranean orchard and garden settings (Rana et al., 2019), but rather the temporal mismatch between newly established plantings and the radiative service they are intended to provide. Comparative reviews emphasise that pedestrian-level cooling efficacy is governed by structural traits such as canopy diameter, leaf area density, and the lateral offset between the trunk and the area to be shaded, rather than by species presence alone (Francini et al., 2023; Rötzer et al., 2024; Stratópoulos et al., 2024).

For Mediterranean school playgrounds, this implies that vegetation audits must explicitly evaluate current canopy geometry at pedestrian scale and incorporate the time horizon required for plantings to deliver effective shade, a delay of 5-15 years for most broadleaved species (Li et al., 2024). In the specific case of ESJF, the Orangery POI thus signals a planting that is functionally promising but operationally premature: the trees will, in time, contribute to the radiative budget, but at present they do not modify pedestrian-level exposure and cannot be counted as an active mitigation element in the schoolyard.

5.4. Ground surface temperatures and the cutaneous burn risk

The simulated T_s profiles add a public-health dimension that is absent from purely T_a- or UTCI-based analyses. The Sports Field and Sports Court, the two surfaces over which student recreation is effectively concentrated, exceed the 55 °C ASTM C1055-20 cutaneous burn-risk threshold for three consecutive hours (12:00-14:00). At these temperatures, contact-burn injuries can occur within seconds of brief barefoot contact or direct sitting on the ground (Pfautsch & Wujeska-Klause, 2022). The fact that the threshold is breached on a representative warm spring day strongly suggests that the threshold is exceeded across a substantial fraction of the school year, particularly given the documented intensification and lengthening of Iberian heatwaves (Bento et al., 2025; EUMETSAT, 2026; Sánchez-Benítez et al., 2025).

On the other hand, surfaces beneath the Loquat and Linden canopies remain below 37 °C throughout the day, tracking ambient T_a closely. The 22 °C T_s differential at 14:00 between the Sports Court and the Loquat canopy quantifies, in absolute physical terms, the protective value of dense deciduous shade. This finding directly extends the Cordeiro et al. (2025) recommendation to expand tree cover in "high-exposure areas" by attaching to it a measurable safety justification: the question is no longer only one of comfort but of avoiding preventable, behaviourally plausible burn injuries among adolescents. Independent measurements in Parisian, Barcelonian, and North-American school playgrounds have reported analogous threshold exceedances, motivating large-scale asphalt-removal programmes in Los Angeles, Philadelphia, and the Trust for Public Land partner districts (Sanz-Mas et al., 2025; Vanos et al., 2024).

5.5. Beyond the simple SVF metric: morphology and longwave traps

An important methodological insight emerges from the anomalous behaviour of the Shed. Despite a comparatively low SVF (0.42) – which would intuitively suggest substantial sky obstruction and thus radiative protection – the location accumulates 2 hours of very strong heat stress and registers the highest L_{down} in the entire dataset (517 W/m^2). The overhead structure is not a vegetated canopy but an opaque, heat-storing built element that, while reducing SVF, simultaneously becomes a strong longwave emitter that radiates downward onto the underlying paved surface. This produces a localised longwave "trap" in which the absorbed shortwave is partially re-emitted as longwave radiation incident on pedestrians at close range.

This result echoes the cautionary evidence accumulating in the urban-microclimate literature that SVF, while a useful first-order morphological proxy, is insufficient on its own to predict thermal outcomes (Ge et al., 2026; Lai et al., 2020). Material properties (albedo, emissivity, thermal admittance), ventilation regime, and the horizontal/vertical balance of obstructing elements jointly determine the radiative balance experienced at human level. From a practical standpoint, this implies that the addition of opaque shade structures to school playgrounds must be carefully designed – preferably with reflective upper surfaces, high-albedo materials, ventilation gaps, or vegetated covers (e.g., pergolas with climbing plants) – to avoid replacing one thermal problem with another. Only a hybrid green-grey strategy avoids the longwave-trapping pitfall illustrated here by the Shed.

5.6. Implications for climate-resilient retrofitting of Mediterranean school playgrounds

Bringing the present results together with the perception- and air-temperature-based diagnosis of Cordeiro et al. (2025) yields a coherent, evidence-based portfolio of interventions for ESJF and, by extension, for comparable 20th-century Portuguese secondary schools.

- Open the existing thermal refugia. One of the most cost-effective immediate measures at this site is administrative rather than physical: re-evaluating the access restrictions to the central Garden and the Loquat zone could deliver thermally tolerable recreational space (UTCI < 32 °C) to the entire student body without any physical retrofit.

- Targeted asphalt-to-canopy conversion in the eastern recreation sector. Strategically planted clusters of broadleaved deciduous trees (e.g., *Tilia cordata*, *Celtis australis*, *Platanus hispanica*) along the eastern edge of the Sports Field and around the Sports Court would directly address the burn-risk hotspots. Recent scenario simulations indicate that converting impervious to canopy cover yields among the highest aggregated UTCI reductions of any urban greening strategy (Li et al., 2024; Yi et al., 2025).

- Cool-pavement and unsealing measures as transitional actions. While newly planted trees take 5-15 years to provide effective shade, immediate relief can be obtained through high-albedo pavement coatings or, where structurally feasible, full unsealing and replacement with permeable, biosourced surfaces. Recent monitored interventions in the OASIS Paris programme report T_s reductions of 10-15 °C and meaningful improvements in pedestrian heat stress under such strategies (Bouyer et al., 2024).

- Hybrid shade structures, not opaque sheds. Following the longwave-trap evidence at the Shed POI, any built-shade addition should preferentially take the form of vegetated pergolas, light-permeable canopies, or tensile sails with high upper albedo, ventilated above to dissipate stored longwave radiation.

- Connection with the broader urban green network. As noted in Cordeiro et al. (2025), ESJF lies within a few hundred metres of the Jardim da Sereia, the "Liceu" garden, also designed by Carlos Ramos along with ESJF, and the Botanical Garden of the University of Coimbra. Aligning species selection and planting strategy with these adjacent green elements would extend cooling beyond the campus, support pollinator and bird connectivity, and contribute to citywide UHI mitigation in line with European Green Deal targets.

- Co-design and maintenance. Technical interventions deliver durable benefits only when paired with stewardship. Consistent with the participatory framework of Cordeiro et al. (2025) and Sanz-Mas et al. (2025), the integration of student-led "green brigades", garden-based curriculum modules, and routine pruning protocols would protect the radiative performance of canopies over time and convert the schoolyard into a living laboratory for climate adaptation.

5.7. Limitations and future research

Several limitations should be acknowledged. First, the simulations are based on a single representative clear-sky day (9 May 2024), selected to maximise radiative contrast under anticyclonic conditions; the results should therefore be read as indicative of upper-bound spatial gradients rather than annual averages. Multi-day or seasonal simulations would refine the estimation of cumulative exposure. Second, SOLWEIG, despite its physical rigour, simplifies the representation of canopy transmissivity and does not explicitly resolve transpirational latent-heat fluxes from individual trees, which can lead to conservative cooling estimates relative to coupled canopy-energy-balance models (Gholami et al., 2024). Third, T_s values were derived from upwelling longwave under a fixed emissivity assumption; field validation with infrared thermography would strengthen the burn-risk diagnosis. Fourth, although the regression $UTCI = 15.43 + 0.349 \cdot T_{mrt}$ is robust across the present dataset, its slope and intercept depend on the prevailing Ta-RH-wind regime and should not be transposed mechanically to other Mediterranean sites.

Future work should pursue three complementary directions. First, longitudinal multi-day SOLWEIG runs forced by ERA5 or Copernicus C3S reanalysis would quantify the annual fraction of school hours spent above each UTCI threshold under current and projected climates, building on the recent CMIP6/EURO-CORDEX projections for the Iberian Peninsula (Bento et al., 2025; Sánchez-Benítez et al., 2025). Second, scenario simulations of the proposed interventions (canopy expansion, asphalt unsealing, pergolas with climbers) would allow ex-ante evaluation of their cooling potential and inform prioritisation, in line with the "before-after" modelling logic now standard in the field (Yi et al., 2025). Third, coupling these radiative outputs with student physiological measurements and behavioural mapping would close the loop between modelled thermal exposure, perceived comfort, and observed activity patterns: research agenda explicitly called for in recent reviews of children-specific outdoor thermal comfort (Vanos, 2015; Zheng et al., 2024).

5.8. Theoretical contribution: towards a geographical reading of the urban microclimate

Despite the empirical robustness of the results, this study advances a set of theoretical contributions relevant to urban physical geography and to climatology applied to spatial planning, moving beyond the mere quantification of microclimatic patterns.

First, the findings consolidate the notion that the radiative environment is the primary driver of thermal stress in outdoor urban spaces, particularly under clear-sky Mediterranean conditions. Demonstrating this relationship at a micro-spatial scale (0.3 m), within a specific functional context such as a schoolyard, enables a scalar reinterpretation of the Urban Heat Island (UHI). Traditionally analysed at the urban or mesoscale, the UHI is here expressed as a hyper-local and functional phenomenon, with substantial thermal gradients occurring within a single institutional setting.

This leads to the formulation of the concept of a functional micro-urban heat island; understood as a localized thermal system whose intensity depends not only on urban morphology but also on the spatial organization of uses and accessibility regimes. In the case examined, the concentration of users in the most exposed areas amplifies the effective thermal load experienced, highlighting that thermal comfort is shaped not only by biophysical factors but also by institutional and behavioural dynamics.

Within this framework, the study introduces the concept of a thermal accessibility paradox, defined as the mismatch between the physical availability of thermally favourable spaces and their actual use. This paradox suggests that the effectiveness of nature-based solutions does not depend solely on their physical presence, but also on their integration into patterns of use and spatial governance.

A third contribution emerges from the analysis of urban vegetation. The results show that the mere presence of trees does not guarantee thermal benefits; rather, what is decisive is the effective canopy geometry at pedestrian level. This supports a distinction between the structural presence and the radiative functionality of vegetation, emphasizing the importance of canopy maturity, density, and spatial configuration in delivering ecosystem services. This perspective introduces a temporal dimension that is often overlooked in green infrastructure planning.

Furthermore, the thermal behaviour of built structures highlights the limitations of the SVF as a standalone indicator of thermal comfort. While useful as a morphological metric, SVF does not adequately capture the effects of longwave radiation re-emission from built surfaces. A more comprehensive approach is therefore required, integrating urban geometry, material properties, and energy balance.

Finally, the study contributes to the consolidation of what may be termed an operational urban climatology, in which microclimatic modelling evolves from a diagnostic tool into a direct support instrument for spatial planning. By translating complex physical variables (T_{mrt}, UTCI, T_s) into metrics relevant to well-being and safety (such as burn risk and thermal stress thresholds), the study reinforces the link between scientific knowledge and territorial decision-making.

6. Conclusions

This study applied the SOLWEIG microclimatic modelling framework to evaluate outdoor thermal comfort and radiative stress at a Mediterranean secondary schoolyard (Escola Secundária José Falcão, Coimbra) on a representative spring day, integrating high-resolution LiDAR-derived morphology, in-situ meteorological forcing, and physically based simulations of T_{mrt}, UTCI, and ground surface temperature.

Three principal findings emerge. (i) Under clear-sky conditions, the radiative environment – captured by T_{mrt} – explains 94% of the spatial variability in UTCI across the schoolyard, whereas air temperature is quasi-uniform; in-situ T_a measurements are therefore necessary as boundary forcing but insufficient to characterise pedestrian-level heat exposure. (ii) The schoolyard exhibits a strong thermal dichotomy: the most thermally favourable areas (dense Loquat and Linden canopies, central Garden) are precisely those that institutional policy renders inaccessible to students, who are thereby concentrated in the most radiatively hostile sector of the campus; the asphalt Sports Field and Sports Court accumulate up to 11 hours of strong-to-very-strong heat stress and exceed the 55 °C ASTM C1055-20 cutaneous burn-risk threshold for three consecutive hours around midday. (iii) Cooling efficacy is governed by mature canopy size and pedestrian-level shadow fraction, not by tree presence alone; the Orangery POI, where young orange trees have not yet developed crowns large enough to shade the adjacent paved area, illustrates the temporal gap between planting and effective radiative service, while the Shed shows how opaque built-shade structures can paradoxically increase downward longwave loading.

Methodologically, the study demonstrates the added value of coupling perception- and air-temperature-based assessments – such as those reported in Cordeiro et al. (2025) for the same school – with physically based radiative modelling. The two layers are not redundant but complementary: surveys and T_a measurements diagnose the boundary conditions and the user experience, while SOLWEIG resolves the underlying radiative mechanisms with metric-scale spatial precision. Together, they provide a robust, mechanistically grounded basis for designing climate-adaptive retrofits.

Practically, the results support a hybrid green-grey adaptation strategy combining (a) the immediate opening of existing thermal refugia, (b) targeted asphalt-to-canopy conversion in the eastern recreation sector with broadleaved deciduous species, (c) cool-pavement coatings as transitional measures, (d) vegetated shade structures designed to avoid longwave traps, and (e) integration with Coimbra's broader green-infrastructure network. Implemented through participatory co-design and supported by stewardship programmes, such interventions can simultaneously address comfort, safety, well-being, and educational mission – reinforcing the role of school playgrounds as nodes of urban climate resilience and as living laboratories for sustainability in line with SDG 3, 4, 11, and 13 and the European Green Deal.

References

Antoniadis, D., Katsoulas, N., & Papanastasiou, D. K. (2020). Thermal environment of urban schoolyards: Current and future design with respect to children's thermal comfort. *Atmosphere*, *11*(11), 1144. https://doi.org/10.3390/atmos11111144

Aroso, S., Cordeiro, A., & Lameiras, J. (2026). Green spaces: Urban heat island mitigation and building climate resilience in coimbra. *Atmosphere*, *17*(3), 284. https://doi.org/10.3390/atmos17030284

ASTM International. (2020). ASTM C1055-20: Standard guide for heated system surface conditions that produce contact burn injuries. *ASTM International*. https://www.astm.org/c1055-20.html

Bento, V. A., Lima, D. C. A., Santos, L. L., et al. (2025). Projections of population exposure to hot and dry events in the end of the 21st century on the iberian peninsula. *Frontiers in Climate*, *7*, 1519880. https://doi.org/10.3389/fclim.2025.1519880

Bouyer, J., Musy, M., Demazeux, J., & Dunand, F. (2024). Thermal and microclimatic behaviour of OASIS schoolyard paving materials. *arXiv preprint arXiv:2408.08317*. https://arxiv.org/abs/2408.08317

Bröde, P., Fiala, D., Błażejczyk, K., Holmér, I., Jendritzky, G., Kampmann, B., Tinz, B., & Havenith, G. (2012). Deriving the operational procedure for the universal thermal climate index (UTCI). *International Journal of Biometeorology*, *56*(3), 481–494. https://doi.org/10.1007/s00484-011-0454-1

Coelho, C., Cordeiro, A., Alcoforado, L., & Moniz, G. C. (2022). Survey on student school spaces: An inclusive design tool for a better school. *Buildings*, *12*(4), 392. https://doi.org/10.3390/buildings12040392

Cordeiro, A., Ornelas, A., & Lameiras, J. (2023). The thermal regulator role of urban green spaces: The case of coimbra (portugal). *Forests*, *14*(12), 2351. https://doi.org/10.3390/f14122351

Cordeiro, A. M. R., Fialho, J., Coelho, C., & Lameiras, J. M. (2025). Greening schools for climate resilience and sustainable co-design: A case study of thermal comfort in coimbra, portugal. *Land*, *14*(10), 1985. https://doi.org/10.3390/land14101985

Cos, J., Doblas-Reyes, F., Jury, M., Marcos, R., Bretón-López, P. A., & Lledo, L. (2024). Recent heatwaves as a prelude to climate extremes in the western mediterranean region. *npj Climate and Atmospheric Science*, *7*, 218. https://doi.org/10.1038/s41612-024-00763-6

DGT. (2023). Ortofotomapas digitais de portugal continental (resolução 0,3 m) [Data set. Direção-Geral do Território]. https://www.dgterritorio.gov.pt/

Di Napoli, C., Hogan, R. J., & Pappenberger, F. (2024). Mean radiant temperature from global-scale numerical weather prediction models. *International Journal of Biometeorology*, *68*(3), 547–559. https://doi.org/10.1007/s00484-023-02597-y

EUMETSAT. (2026, April). Europe in 2025: Extremes from the arctic circle to the mediterranean. *European Organisation for the Exploitation of Meteorological Satellites*. https://www.eumetsat.int/features/europe-2025-extremes-arctic-circle-mediterranean

Ferreira, D. B. (2005). O ambiente climático. In C. A. Medeiros (Ed.), *Geografia de portugal: Ambiente físico* (Vol. 1). Círculo de Leitores.

Francini, A., Toscano, S., Ferrante, A., & Romano, D. (2023). Method for selecting ornamental species for different shading intensity in urban green spaces. *Frontiers in Plant Science*, *14*, 1271341. https://doi.org/10.3389/fpls.2023.1271341

Ge, X., Wang, Y., Liu, J., & Chen, L. (2026). Passive climate adaptation of heritage arcades: Field evidence on the geometry-radiation-thermal comfort chain and orientation effects. *Buildings*, *16*(1), 201. https://doi.org/10.3390/buildings16010201

Gholami, M., Barbaresi, A., Tassinari, P., & Torreggiani, D. (2024). A python-based mean radiant temperature and UTCI calculation approach for thermal stress assessment. *Building and Environment*, *248*, 111054. https://doi.org/10.1016/j.buildenv.2023.111054

Höppe, P. (1999). The physiological equivalent temperature - a universal index for the biometeorological assessment of the thermal environment. *International Journal of Biometeorology*, *43*(2), 71–75. https://doi.org/10.1007/s004840050118

Huld, T., Müller, R., & Gambardella, A. (2012). A new solar radiation database for estimating PV performance in europe and africa. *Solar Energy*, *86*(6), 1803–1815. https://doi.org/10.1016/j.solener.2012.03.006

IPCC. (2023). *Climate change 2023: Synthesis report. contribution of working groups i, ii and iii to the sixth assessment report of the intergovernmental panel on climate change* (Core Writing Team, H. Lee, & J. Romero, Eds.; tech. rep.). IPCC. https://doi.org/10.59327/IPCC/AR6-9789291691647

Jänicke, B., Meier, F., Lindberg, F., Schubert, S., & Scherer, D. (2024). Towards a more realistic representation of urban surface temperatures in microclimate models. *Urban Climate*, *53*, 101803. https://doi.org/10.1016/j.uclim.2023.101803

Jézéquel, A., Vautard, R., & Yiou, P. (2025). Extreme event attribution in the mediterranean. *International Journal of Climatology*, *45*(2), e8799. https://doi.org/10.1002/joc.8799

Kántor, N., & Unger, J. (2011). The most problematic variable in the course of human-biometeorological comfort assessment - the mean radiant temperature. *Central European Journal of Geosciences*, *3*(1), 90–100. https://doi.org/10.2478/s13533-011-0010-x

Konarska, J., Lindberg, F., Larsson, A., Thorsson, S., & Holmer, B. (2024). Transmissivity of solar radiation through crowns of single urban trees and the impact on radiative load and thermal comfort. *Theoretical and Applied Climatology*, *156*, 197–215. https://doi.org/10.1007/s00704-024-04999-3

Lai, D., Lian, Z., Liu, W., Guo, C., Liu, W., Liu, K., & Chen, Q. (2020). A comprehensive review of thermal comfort studies in urban open spaces. *The Science of the Total Environment*, *742*, 140092. https://doi.org/10.1016/j.scitotenv.2020.140092

Li, H., Zhao, Y., Wang, C., Ürge-Vorsatz, D., Carmeliet, J., & Bardhan, R. (2024). Cooling efficacy of trees across cities is determined by background climate, urban morphology, and tree trait. *Communications Earth & Environment*, *5*(1), 754. https://doi.org/10.1038/s43247-024-01908-4

Lima, D. C. A., Bento, V. A., Lemos, G., Nogueira, M., & Soares, P. M. M. (2023). A multi-variable constrained ensemble of regional climate projections under multi-scenarios for portugal – part ii: Sectorial climate indices. *Climate Services*, *30*, 100377. https://doi.org/10.1016/j.cliser.2023.100377

Lindberg, F., & Grimmond, C. S. B. (2011). The influence of vegetation and building morphology on shadow patterns and mean radiant temperatures in urban areas: Model development and evaluation. *Theoretical and Applied Climatology*, *105*(3), 311–323. https://doi.org/10.1007/s00704-010-0382-8

Lindberg, F., Grimmond, C. S. B., Gabey, A., Huang, B., Kent, C. W., Sun, T., Theeuwes, N. E., Järvi, L., Ward, H. C., Capel-Timms, I., Chang, Y., Jonsson, P., Krave, N., Liu, D., Meyer, D., Olofson, K. F. G., Tan, J., Wästberg, D., Xue, L., & Zhang, Z. (2018). Urban multi-scale environmental predictor (UMEP): An integrated tool for city-based climate services. *Environmental Modelling & Software*, *99*, 70–87. https://doi.org/10.1016/j.envsoft.2017.09.020

Lindberg, F., Holmer, B., & Thorsson, S. (2008). SOLWEIG 1.0 - modelling spatial variations of 3d radiant fluxes and mean radiant temperature in complex urban settings. *International Journal of Biometeorology*, *52*(7), 697–713. https://doi.org/10.1007/s00484-008-0162-7

Massetti, L., Petralli, M., Napoli, M., Brandani, G., Orlandini, S., & Pearlmutter, D. (2019). Effects of deciduous shade trees on surface temperature and pedestrian thermal stress during summer and autumn. *International Journal of Biometeorology*, *63*(4), 467–479. https://doi.org/10.1007/s00484-019-01679-0

MedECC. (2020). *Climate and environmental change in the mediterranean basin - current situation and risks for the future. first mediterranean assessment report* (W. Cramer, J. Guiot, & K. Marini, Eds.; tech. rep.). Union for the Mediterranean, Plan Bleu, UNEP/MAP. https://www.medecc.org/medecc-reports/climate-and-environmental-change-in-the-mediterranean-basin-current-situation-and-risks-for-the-future-1st-mediterranean-assessment-report/

Moniz, G. C. (2007). *Arquitectura e instrução: Projecto moderno de liceu (1836-1936)*. Edições Almedina/EDARQ.

Nouri, A. S., Costa, J. P., Santamouris, M., & Matzarakis, A. (2024). Approaches to outdoor thermal comfort thresholds through public space design: A review. *Atmosphere*, *15*(7), 783. https://doi.org/10.3390/atmos15070783

Nóvoa, A. S. (2003). *Liceus de portugal: Histórias, arquivos, memórias*. Edições Asa.

Pfautsch, S., & Wujeska-Klause, A. (2022). Hot playgrounds: A systematic review of the surface temperatures of playground equipment. *Building and Environment*, *219*, 109229. https://doi.org/10.1016/j.buildenv.2022.109229

Pioppi, B., Pisello, A. L., Ramamurthy, P., & Salvati, A. (2024). Bridging outdoor thermal comfort modelling and field campaigns: A wearable-sensor approach in mediterranean urban environments. *Building and Environment*, *248*, 111107. https://doi.org/10.1016/j.buildenv.2023.111107

Presidência do Conselho de Ministros. (2007). Resolução do conselho de ministros n.º 1/2007, de 3 de janeiro: Aprova o programa de modernização do parque escolar destinado ao ensino secundário.

Rahman, M. A., Moser, A., Rötzer, T., & Pauleit, S. (2017). Microclimatic differences and their influence on transpirational cooling of tilia cordata in two contrasting street canyons in munich, germany. *Agricultural and Forest Meteorology*, *232*, 443–456. https://doi.org/10.1016/j.agrformet.2016.10.006

Rana, G., Pellegrino, A., Ferrara, R. M., & Martinelli, N. (2019). Tree transpiration in a multi-species mediterranean garden. *Agricultural and Forest Meteorology*, *280*, 107767. https://doi.org/10.1016/j.agrformet.2019.107767

Riaz, H., Riaz, A., Iqbal, A., Amina, N., & Imtiaz, S. (2025). A review on significance of thermal comfort in educational facilities. *Building Engineering*, *3*(2), 2100. https://doi.org/10.59400/be2100

Rötzer, T., Moser-Reischl, A., Rahman, M. A., Hartmann, C., Paeth, H., Pauleit, S., & Pretzsch, H. (2024). Within canopy temperature differences and cooling ability of urban trees grown under contrasting site conditions. *Environmental and Experimental Botany*, *227*, 105943. https://doi.org/10.1016/j.envexpbot.2024.105943

Sánchez-Benítez, A., Vicente-Serrano, S. M., Beguería, S., & Trigo, R. M. (2025). Heat and cold wave intensity and spatial extent on the iberian peninsula: Future climate projections (2050-2095). *Climate Dynamics*, *63*, 1–22. https://doi.org/10.1007/s00382-025-07699-4

Santamouris, M., Synnefa, A., & Karlessi, T. (2011). Using advanced cool materials in the urban built environment to mitigate heat islands and improve thermal comfort conditions. *Solar Energy*, *85*(12), 3085–3102. https://doi.org/10.1016/j.solener.2010.12.023

Sanz-Mas, M., Continente, X., Brugueras, S., Marí-Dell'Olmo, M., Oliveras, L., & López, M. J. (2025). Evaluating the effect of green, blue, and gray measures for climate change adaptation on children's well-being in schoolyards in barcelona. *Landscape and Urban Planning*, *253*, 105206. https://doi.org/10.1016/j.landurbplan.2024.105206

Silva, T., Lopes, A., Vasconcelos, J., Chokhachian, A., Wagenfeld, M., & Santucci, D. (2024). Thermal stress and comfort assessment in urban areas using copernicus climate change service ERA5 reanalysis and collected microclimatic data. *International Journal of Biometeorology*, *68*(5), 949–963. https://doi.org/10.1007/s00484-024-02635-3

Speak, A. F., Montagnani, L., Wellstein, C., & Zerbe, S. (2020). The influence of tree traits on urban ground surface shade cooling. *Landscape and Urban Planning*, *197*, 103748. https://doi.org/10.1016/j.landurbplan.2020.103748

Stratópoulos, L. M. F., Zhang, C., Häberle, K. H., Pauleit, S., Duthweiler, S., Pretzsch, H., & Rötzer, T. (2024). Tree species and size matter: Cooling and shading effects of urban trees during heatwaves in a temperate climate. *Urban Forestry & Urban Greening*, *95*, 128293. https://doi.org/10.1016/j.ufug.2024.128293

UMEP-dev. (2025). SOLWEIG: Solar and longwave environmental irradiance geometry - documentation (2025 release). *UMEP Development Team*. https://umep-dev.github.io/solweig/

Vanos, J. K. (2015). Children's health and vulnerability in outdoor microclimates: A comprehensive review. *Environment International*, *76*, 1–15. https://doi.org/10.1016/j.envint.2014.11.016

Vanos, J. K., Middel, A., Poletti, M. N., & Selover, N. J. (2024). Outdoor thermal comfort, surface temperatures, and heat-mitigation potential of school playgrounds in hot-arid climates. *Building and Environment*, *251*, 111201. https://doi.org/10.1016/j.buildenv.2024.111201

Walikewitz, N., Jänicke, B., Langner, M., Meier, F., & Endlicher, W. (2015). The difference between the mean radiant temperature and the air temperature within indoor environments: A case study during summer conditions. *Building and Environment*, *84*, 151–161. https://doi.org/10.1016/j.buildenv.2014.11.004

Wolf, K. L., Senturia, K., Simmons, C., Hafferty, K., Faino, A. V., Garrett, K. A., & Tandon, P. S. (2024). Participatory design for community schoolyards: Mixed methods reveal positive engagement despite measures limitations. *Ecopsychology*, *16*(2), 113–127. https://doi.org/10.1089/eco.2023.0075

Wong, N. H., Tan, C. L., Kolokotsa, D. D., & Takebayashi, H. (2021). Greenery as a mitigation and adaptation strategy to urban heat. *Nature Reviews Earth & Environment*, *2*(3), 166–181. https://doi.org/10.1038/s43017-020-00129-5

Yang, J., Yang, Y., Sun, D., Jin, C., & Xiao, X. (2021). Influence of urban morphological characteristics on the thermal environment. *Sustainable Cities and Society*, *72*, 103045. https://doi.org/10.1016/j.scs.2021.103045

Yi, S., Li, X., Tu, W., & Zhao, T. (2025, July). Planning for cooler cities: A multimodal AI framework for predicting and mitigating urban heat stress through urban landscape transformation. https://arxiv.org/abs/2507.23000

Zheng, P., Zhang, Z., Liu, J., Zhang, Y., & Lin, Y. (2024). Evaluation methods and factors influencing the thermal comfort of children - a comprehensive literature review. *Journal of Building Engineering*, *91*, 110063. https://doi.org/10.1016/j.jobe.2024.110063